First example of photorelease of nitric oxide from ruthenium nitrosyl-based nanoparticles

Arij Farhat, Marine Tassé, Mathilde Bocé, D de Caro, Isabelle Malfant, Patricia Vicendo, Anne-Françoise Mingotaud

First example of Photorelease of Nitric Oxide from Ruthenium Nitrosyl-based Nanoparticles

Arij Farhat[1], Marine Tassé[1], Mathilde Bocé[1], Dominique de Caro[1]*, Isabelle Malfant[1]*, Patricia Vicendo[2] and Anne-Françoise Mingotaud[2]

1 Laboratoire de Chimie de Coordination du CNRS, 205 route de Narbonne, F-31077 Toulouse, France

2 Laboratoire des IMRCP, Université de Toulouse, CNRS UMR 5623, Université Toulouse III - Paul Sabatier, 118 route de Narbonne, 31062 Toulouse cedex 9, France

Corresponding authors: dominique.decaro@lcc-toulouse.fr; isabelle.malfant@lcc-toulouse.fr

Abstract: We described the facile preparation of nanoparticles of a photoactivable ruthenium nitrosyl complex. Nanoparticle sizes were investigated by atomic force microscopy and nanoparticle tracking analysis. For nanoparticles dispersed in water, nitric oxide (NO) photorelease was evidenced at 365 nm. The quantum yield of photorelease was found to be of about 0.04. Electron paramagnetic resonance as well as measurements by a NO sensor confirmed NO release upon photolysis of nanoparticles. This work showed that these nanoparticles allowed a spatiotemporal control of NO release upon light irradiation and are potential NO nanoplatforms for biological applications.

Keywords: ruthenium nitrosyl complex; nanoparticles; nitric oxide photorelease

1. Introduction

Nitric oxide (NO) is a free-radical gas involved in many physiological and pathological processes [1]. Due to its key role in cellular signaling NO donors such as organic nitrites or nitrates, nitrosothiols, diazeniumdiolates and metal nitrosyl complexes have been developed for therapeutic applications in oncology, infectiology, wound healing, angiology [2-3]. A local control of NO release is essential to avoid side effect. In this context ruthenium nitrosyl (Ru-NO) complexes are of a great interest [4] because they allow to control spatiotemporal release of NO at the biological target site upon their exposure to light while being non-toxic themselves [5]. They exhibit quantum yield of photorelease (ϕ_{NO}) commonly ranging from 0.025 to 0.4, depending on the donor substituent and the wavelength of irradiation [6-9]. In previous experiments, we found that ruthenium nitrosyl complexes with the fluorenyl terpyridine ligand (Fig. 1) were promising candidates for reversing methicillin resistance of *Staphylococcus epidermidis* bacteria [10, 11]. However, many complexes have a poor solubility in biological medium, precipitating in nanoaggregates. To optimize their biodisponibility, cellular uptake and therapeutic outcomes they have been integrated in various drug delivery micro- or nanoplatforms [12-15]. In this context, carrier-free methods for the delivery of hydrophobic photosensitizers have also been developed and proved their efficiency in photodynamic therapy [16]. Such strategy may be applied for hydrophobic Ru-NO complexes. Herein, we report on the synthesis of Ru-NO nanoparticles in aqueous solution starting from *trans*-(Cl,Cl)-[Ru(FT)Cl_2(NO)](PF_6), as well as their characterization and their ability to photorelease NO. To our knowledge, it is the first example of photoactivable RuNO-based nanoparticles.

2. Materials and methods

Trans-(Cl,Cl)-[Ru(FT)Cl_2(NO)](PF_6) (FT: 4'-(2-fluorenyl)-2,2':6',2''-terpyridine) [17] nanoparticles were prepared in the dark by adding dropwise 50 µL of Ru-NO solution (1.04×10^{-3} mol.L^{-1} in acetone) into 5 mL freshly distilled water (GFL Water Still 2004, conductivity 1400 µS.cm^{-1}) for 1, 2 or 4 min. at 25 °C under stirring (350 rpm). After 15 min., a pale-yellow solution was obtained and stored in the dark.

Atomic force microscopy (AFM) was performed using a Smart SPM-100 AIST-NT microscope. Images were acquired in tapping mode (resonance frequency: 325 kHz) with a silicon tip (MikroMasch HQ-NSC15/AlBS). Substrates were (001)-oriented silicon wafers (3 × 10 mm^2) washed with acetone, ethanol, and finally dried under an argon flow. Two drops of nanocrystal solution were deposited onto the silicon substrate and the sample was dried in air.

Nanoparticle Tracking Analysis (NTA) was performed at 25 °C using a NanoSight NS300 equipped with a sCMOS camera (Malvern Instruments, Ltd, UK) instrument. Measurement of each sample in solution in ultrapure Milli-Q water (7.75 mg.L^{-1}) was performed four times, consisting of four records of 60 s.

Photokinetic studies on the photolysis reactions were carried out at 25°C with a Cary 60 UV-Visible spectrophotometer. Irradiation was performed from a chassis wheeled wavelength-switchable LED source from Mightex Company operating at 365 nm with a light intensity of 5 mW. The sample solutions were placed in a quartz cuvette of 1 cm path-length stirred continuously and the optical fiber was fixed laterally from it. The quantum yield (ϕ_{NO}) was determined by the program Sa3.3 [18].

Electron paramagnetic resonance (EPR) spectra were collected on a Brucker ESP 500E (X band) spectrometer. Fe^{2+}-di(*N*-methyl-D-glutamine-dithiocarbamate) was used as NO spin trap.

The quantitative determination of NO production was performed with a commercial NO detector (ami-NO 700) from Innovative Instruments Inc. Calibration of the electrode in the range of 50-1000 nM was performed by generating NO according to the following reaction:

$$2\ NO_2^- + 4\ H^+ + 2\ I^- \rightarrow 2\ NO^{\cdot} + I_2 + 2\ H_2O$$

For each calibration, aliquots (80 µL) of aqueous $NaNO_2$ (~ 100 µM) were added to 20 mL of a 0.03 M solution of KI in 0.1 M H_2SO_4. Chronoamperograms were registered at a fixed temperature (25 °C) while stirring the solution in order to maintain a constant rate of oxidation of the produced NO at the electrode surface. The typical sensitivity of the electrode was about 100 $pA.nM^{-1}$. During the photolysis measurements, the NO sensor was positioned outside the light path. Besides, chronoamperograms of an aqueous solution were systematically registered upon irradiation in order to subtract the light interference. Then, chronoamperograms were registered upon irradiation of 20 mL of an aqueous solution of Ru-NO nanoparticles (400 nM) during 60 s.

3. Results and discussion

3.1. Preparation and size analysis

Terpyridine-based ruthenium nitrosyl nanoparticles were obtained by adding dropwise an acetone solution of *trans*-(Cl,Cl)-[Ru(FT)Cl_2(NO)](PF_6) to water under stirring (dilution factor: 1/100). Three addition times were evaluated, namely 1, 2 and 4 min. AFM images evidenced dispersed nanoparticles (Fig. 2-I). For 1 and 2 min. addition, samples exhibited very similar sizes in the 4–40 nm range, centered on 10 nm (Table 1 and SI, Fig. S1). For 4 min. addition, AFM evidenced a bimodal distribution of sizes (SI, Fig. S1) with a mean size of about 44 nm (Table 1). A first peak was centered at ~32 nm and 2.5 times higher than a second one centered at ~57 nm. NTA showed a trend of decreasing the size with increasing the time of addition (Fig. 2-II and Table 1). One should however keep in mind that NTA lower limit of detection is dependent of the particles analyzed. Inorganic or metallic particles as small as 10 nm can be tracked and analyzed, but soft materials below 50 nm become invisible owing to a too low contrast. Because the lower limit of the peaks obtained here was close to 50 nm, it is therefore possible that NTA only detected the fraction above 50 nm corresponding to the second size peak observed in AFM. Dynamic Light Scattering enabling the detection of smaller nanoparticles was also assessed but the concentration used was below the limit of detection for this technique. Fabricating the nanoparticles at higher concentration could have led to changes of size and morphology, this was thus not performed. Also, increasing the nanoparticles concentration after their formation was not favored, because, in a same manner, this process could have modified them.

3.2. NO photorelease study

In this study, nanoparticles were prepared in the experimental conditions corresponding to an injection time of 1 min. The $NO^{\cdot}$ release capabilities of the nanoparticles were studied upon photolysis at 365 nm (Fig. 3). The wavelength of excitation corresponded to the band of interest as we previously demonstrated to be related to the dominant contribution of the single HOMO-LUMO excitation involving fluorene-Ru(NO) charge transfer [7]. The presence of isosbestic points indicated a clean conversion of the $Ru^{II}(NO^+)$ complexes to photolysed species and no back-reaction was observed when the light was turned off. The ability of ruthenium nitrosyl complexes to release nitric oxide under irradiation was mainly described according to the following chemical equation [8]:

$$(L)Ru^{II}\text{-}(NO^+) + \text{solvent} \xrightarrow{h\nu} (L)Ru^{III}\text{-solvent} + NO^{\cdot}$$

The model used to determine ϕ_{NO} assumed that the starting complex and the final photo-product were the only absorbing species present in solution. For nanoparticles, the value of ϕ_{NO} was found to be 0.041 that is within the range of values for this family of compounds. Moreover, the agreement between the experimental and theoretical points (SI, Table S1 and Fig. S2) strongly supported this description.

An EPR experiment using iron(II)-*N*-methyl-D-glucamine dithiocarbamato, $Fe(MGD)_2$ as NO spin trap [11] was performed to investigate the formation of nitric oxide ($NO^{\cdot}$) during the photolysis of Ru-NO nanoparticles. The EPR spectrum for nanoparticles after 120 min photolysis showed a characteristic triplet signal with a hyperfine splitting constant value of $a_N = 1.2 \times 10^{-3}$ cm^{-1} and a g-factor of g = 2.040 (insert in Fig. 3). This EPR signal was consistent with the formation of the $[(MGD)_2\text{-}Fe^{2+}\text{-}NO]$ complex within the nanoparticles. In the dark, the formation of $NO^{\cdot}$ was not detected supporting the photo-triggered character for the generation of $NO^{\cdot}$. Moreover, direct NO release was confirmed by NO sensor measurements. The chronoamperogram of Ru-NO nanoparticles (400 nM in water) shows clearly a $NO^{\cdot}$ concentration up to 70 nM under irradiation at 365 nm for 60 s (Fig. 4).

4. Conclusions

In this communication, we have described the first nanoparticles of a fluorenylterpyridine-based ruthenium nitrosyl complex prepared in water. They exhibited sizes in the 5-200 nm range. Although their size was not properly controlled, the synthetic method we described here was very simple and was carried out under mild conditions. Moreover, for the lowest addition rate of the Ru-NO complex to water (*i.e.*, 1 min.), near-field micrographs showed nanoparticles exhibiting a very good state of dispersion. Under irradiation at 365 nm, nanoparticles were shown to release NO as a neutral radical, which is a point in favor of potential applications. These nanoparticles can thus be considered as nanoplatforms for NO delivery for anticancer photodynamic therapy or as antibacterial agents.

References

1- J.O. Lundberg, E. Weitzberg, Nitric oxide signaling in health and disease, Cell 18 (2022) 2853–2878. https://doi.org/10.1016/j.cell.2022.06.010
2- P.G. Wang, M. Xian, X. Tang, X. Wu, Z. Wen, T. Cai, A.J. Janczuk, Nitric oxide donors: chemical activities and biological applications, Chem. Rev. 102 (2002) 1091–1134. https://doi.org/10.1021/cr000040l
3- Y. Yang, Z. Huang, L.L. Li, Advanced nitric oxide donors: chemical structure of NO drugs, NO nanomedicines and biomedical applications, Nanoscale 13 (2021) 444–459. https://doi-org-s.docadis.univ-tlse3.fr/10.1039/D0NR07484E
4- T.R. deBoer, P.K. Mascharak, Recent progress in photoinduced NO delivery with designed ruthenium nitrosyl complexes, in: R. van Eldik, J.A. Olabe (Eds.), Advances in Inorganic Chemistry, Elsevier Inc., Waltham, 2015, pp. 145–170. https://doi-org-s.docadis.univ-tlse3.fr/10.1016/bs.adioch.2014.11.002
5- I. Stepanenko, M. Zalibera, D. Schaniel, J. Telser, V.B. Arion, Ruthenium-nitrosyl complexes as NO-releasing molecules, potential anticancer drugs, and photoswitches based on linkage isomerism, Dalton Trans. 51 (2022) 5367–5393. https://doi:10.1039/d2dt00290f
6- S.R. Wecksler, J. Hutchinson, P.C. Ford, Toward development of water soluble dye derivatized nitrosyl compounds for photochemical delivery of NO, Inorg. Chem. 45 (2006) 1192–1200. https://doi.org/10.1021/ic051723s

7- J. Akl, I. Sasaki, P.G. Lacroix, I. Malfant, S. Malet-Ladeira, P. Vicendo, N. Farfán, R. Santillan, Comparative photo-release of nitric oxide from isomers of substituted terpyridinenitrosylruthenium(II) complexes: experimental and computational investigations, Dalton Trans. 43 (2014) 12721–12733. https://doi.org/10.1039/C4DT00974F
8- N.L. Fry, P.K. Mascharak, Photoactive ruthenium nitrosyls as NO donors: How to sensitize them toward visible light, Acc. Chem. Res. 44 (2011) 289–298. https://doi.org/10.1021/ar100155t
9- S. Amabilino, M. Tassé, P.G. Lacroix, S. Mallet-Ladeira, V. Pimenta, J. Akl, I. Sasaki, I. Malfant, Photorelease of nitric oxide (NO) on ruthenium nitrosyl complexes with phenyl substituted terpyridines, New J. Chem. (41) 2017, 7371–7383. https://doi.org/10.1039/C7NJ00866J
10- J. Akl, I. Sasaki, P.G. Lacroix, V. Hugues, P. Vicendo, M. Bocé, S. Mallet-Ladeira, M. Blanchard-Desce, I. Malfant, *Trans*- and *cis*-(Cl,Cl)-[Ru^{II}(FT)Cl_2(NO)](PF_6): promising candidates for NO release in the NIR region, Photochem. Photobiol. Sci. 15 (2016) 1484–1491. https://doi.org/10.1039/C6PP00181E
11- M. Bocé, M. Tassé, S. Mallet-Ladeira, F. Pillet, C. Da Silva, P. Vicendo, P.G. Lacroix, I. Malfant, M. P. Rols, Effect of *trans*-(NO, OH)-[RuFT(Cl)(OH)NO](PF_6) ruthenium nitrosyl complex on methicillin resistant *Staphylococcus epidermidis*, Sci. Rep. 9 (2019) 4867–4874. https://doi.org/10.1038/s41598-019-41222-0
12- S. Kumar, R. Kumar, A. Ratnam, N.C. Mishra, K. Ghosh, Novel drug delivery system for photoinduced nitric oxide (NO) delivery, Inorg. Chem. Comm. 53 (2015) 23–25. http://dx.doi.org/10.1016/j.inoche.2015.01.013
13- H.J. Xiang, M. Guo, J.G. Liu, Transition metal nitrosyls for photocontrolled nitric oxide delivery, Eur. J. Inorg. Chem. (2017) 1586–1595. https://doi.org/10.1002/ejic.201601135
14- A.J. Gomes, P.A. Barbougli, E.M. Espreafico, E. Tfouni, *Trans*-[Ru(NO)(NH_3)$_4$(py)](BF_3)$_4$·H_2O encapsulated in PLGA microparticles for delivery of nitric oxide to B16-F10 cells: cytotoxicity and phototoxicity, J. Inorg. Biochem. 102 (2008) 757–766. https://doi.org/10.1016/j.jinorgbio.2007.11.012
15- C.H. Ho, K.J. Liao, C.N. Lok, C.M. Che, Nitric oxide-releasing ruthenium nanoparticles, Chem. Commun. 47 (2011) 10776–10778. 10.1039/C1CC13830H
16- F.-F. An, Y. Li, J. Zhang, Carrier-free photosensitizer nanocrystal for photodynamic therapy, Material Letters 122 (2014) 323–326. https://doi.org/10.1016/j.matlet.2014.02.067
17- P. Labra-Vázquez, M. Bocé, M. Tassé, S. Mallet-Ladeira, P.G. Lacroix, N. Farfán, I. Malfant, Chemical and photochemical behavior of ruthenium nitrosyl complexes with terpyridine ligands in aqueous media, Dalton Trans. 49 (2020) 3138–3154. https://doi.org/10.1039/C9DT04832D
18- Program Sa3.3 written by D. Lavabre and V. Pimenta. The software can be downloaded at http://cinet.chim.pagesperso-orange.fr/

Figure captions:

Figure 1. Molecular formula for *trans*-(Cl,Cl)-[Ru(FT)Cl_2(NO)](PF_6).

Figure 2. I- AFM topographic images for Ru-NO nanoparticles: 1 min. (A), 2 min. (B), 4 min. (C) addition. II- NTA of the solutions of Ru-NO nanoparticles: 1 min. (A), 2 min. (B), 4 min. (C) addition.

Figure 3. Evolution in the absorption spectra of Ru-NO nanoparticles in H_2O (1 min. addition) under irradiation at λ = 365 nm. Blue line: before irradiation, red line: after 15 minutes irradiation. Insert: Triplet EPR signals NO-[$Fe(MGD)_2$] adduct upon irradiation of Ru-NO nanoparticles at λ = 365 nm (red line) and room temperature for 120 min. Blue line: control before irradiation.

Figure 4. Chronoamperograms of Ru-NO nanoparticles (1 min. addition) at a concentration of 400 nM in H_2O under irradiation of 60 s at λ = 365 nm (arrow at t = 0 s). The typical sensitivity of the NO detector was 106 pA.nM^{-1}.

Table:

Table 1. Size of Ru-NO nanoparticles obtained from AFM and NTA. Results are given as a mean ± standard deviation.

Figure 1:

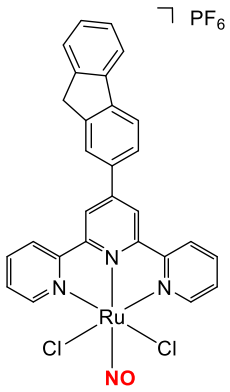

Figure 2:

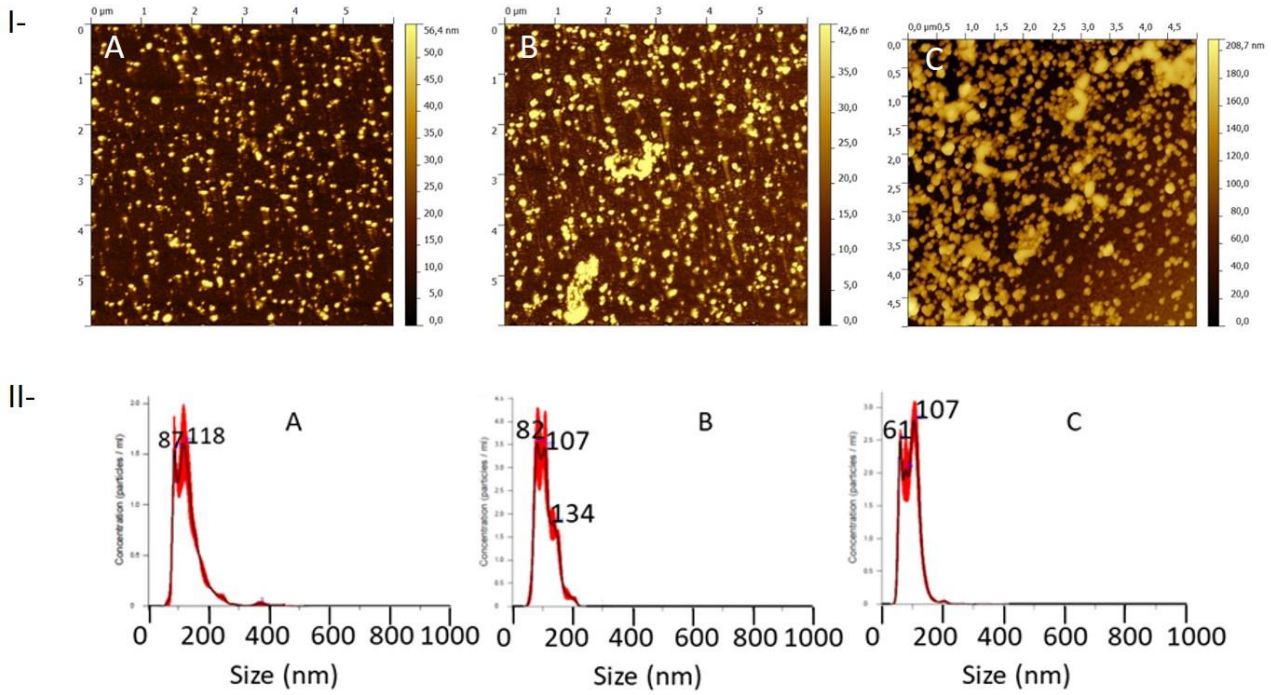

Figure 3:

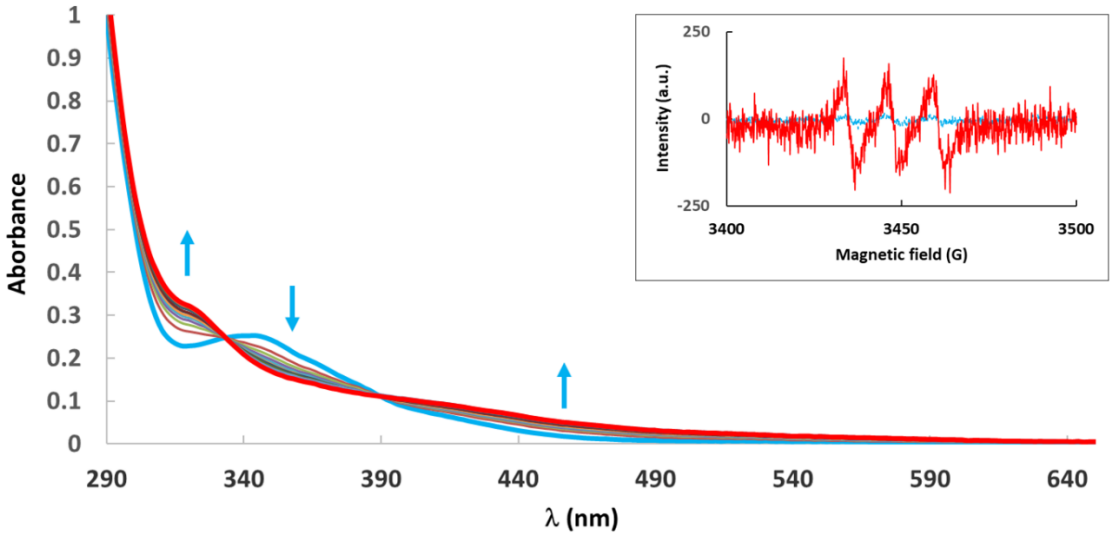

Figure 4:

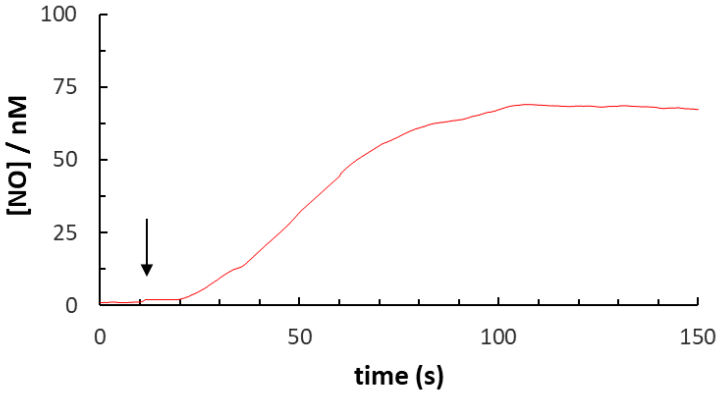

Table 1:

Time of addition	Size from AFM (nm)	Size from NTA (nm)
1 min.	16.2 ± 4.5	133 ± 49
2 min.	16.0 ± 4.5	110 ± 30
4 min.	44.3 ± 16.3	95 ± 27

Supporting information

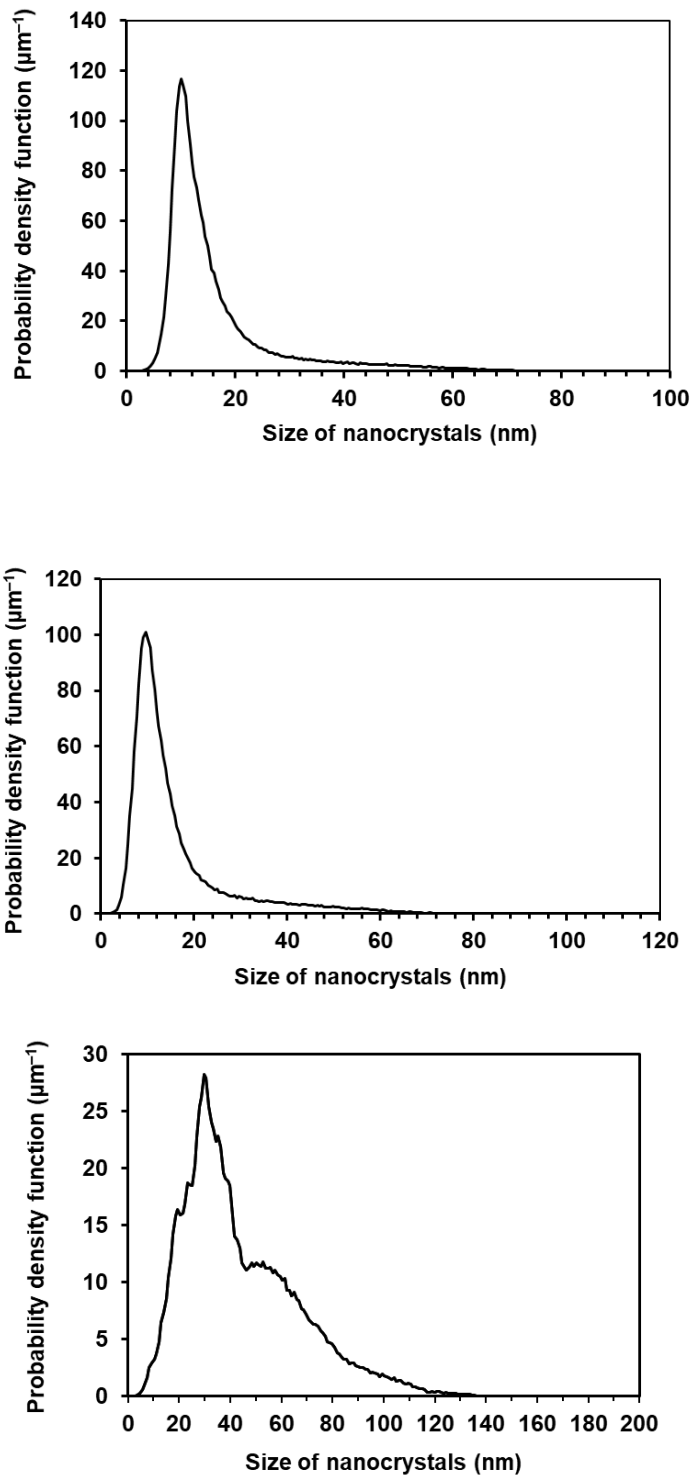

Fig. S1. Size distributions from AFM images: 1 min. (top), 2 min. (middle), 4 min. (down) addition for a dilution factor of 1/100.

λ_{irr} = 365 nm λ_{obs} = 320 nm	Ru-NO nanoparticles (dilution factor 1/100; 1 min. addition)
Φ_{NO}^{irr}	0.041
I_0 (mol.L^{-1}.s^{-1})	8.01×10^{-6}
$[A]_{initial}$ (mol.L^{-1})	1.04×10^{-5}
$[B]_{final}$ (mol.L^{-1})	1.04×10^{-5}
ε_A^{irr} (mol^{-1}.L.cm^{-1})	18077
ε_A^{obs} (mol^{-1}.L.cm^{-1})	22115
ε_B^{irr} (mol^{-1}.L.cm^{-1})	14029
ε_B^{obs} (mol^{-1}.L.cm^{-1})	29825

Table S1. Experimental data for the determination of Φ_{NO}^{irr} for Ru-NO nanoparticles in H_2O (dilution factor 1/100; 1 min. addition) at λ_{irr} = 365 nm.

Kinetic model for quantum yield calculation

Quantum yield measurements: Light intensity (I_0) was determined before the photolysis experiments. The quantum yield (ϕ_{NO}) was determined by the program Sa3.3 written by D. Lavabre and V. Pimienta (reference 18). It allows the resolution of the differential equation (1):

$$\frac{d[A]}{dt} = -\Phi_{NO}\, I_a^A = -\Phi_{NO}\, Abs_A^{\lambda} I_0 F \qquad (1)$$

where I_a^A is the intensity of the light absorbed by the precursor; Abs_A^{λ} , the absorbance before irradiation; Abs_{Tot}^{λ}, the total absorbance; I_0, the incident intensity measured at 365 nm; and F, the photokinetic factor given by equation (2):

$$F = \frac{\left(1-10^{-Abs_{Tot}^{\lambda}}\right)}{Abs_{Tot}^{\lambda}} \qquad (2)$$

The equation was fitted with the experimental data $Abs_{Tot}^{\lambda} = f(t)$ and 2 parameters ϕ_{NO} and ε_B (ε_B is the molar extinction coefficient measured at the end of the reaction) at two wavelengths (λ_{irr} = 365 nm, λ_{obs} = 320 nm). λ_{obs} was chosen because it corresponds to a large difference between molar extinction coefficient at the initial and final time of the photochemical reaction. Simulation and optimization procedures were performed by using numerical integration and a non-linear minimization algorithm for the fitting of the model to the experimental data (reference 18).

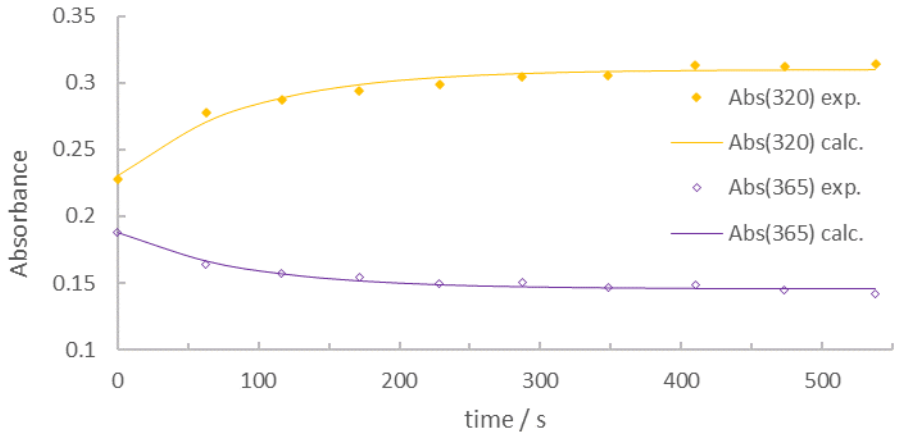

Fig. S2. Experimental and calculated absorbance for Ru-NO nanoparticles in H_2O (volume dilution factor 1/100; 1 min. addition) for λ_{irr} = 365 nm (purple) and λ_{obs} = 320 nm (orange). R (correlation coefficient of Pearson) is equal to 0.9990.